Heliyon 9 (2023) e19004

Contents lists available at ScienceDirect

Heliyon

journal homepage: www.cell.com/heliyon

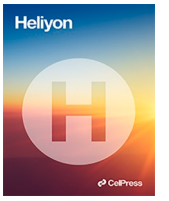

Significance of improved heat conduction on unsteady axisymmetric flow of Maxwell fluid with cubic autocatalysis chemical reaction

Muhammad Yasir [a,*], Masood Khan [*,a], Asia Anjum [b], M. Munawwar Iqbal Ch [c]

[a] Department of Mathematics, Quaid-i-Azam University, Islamabad, 44000, Pakistan
[b] Department of Computer Science, National University of Modern Languages, H-9, Islamabad, Pakistan
[c] Institute of Information Technology, Quaid-i-Azam University, Islamabad, 44000, Pakistan

ARTICLE INFO

Keywords:
Maxwell fluid
Stretching cylinder
Cubic autocatalysis chemical reaction
Cattaneo-Christov heat transport
Magnetic field

ABSTRACT

This paper investigates the effect of chemical reactions on the flow of magnetized Maxwell fluid generated by an unsteady stretching surface. The thermal transport phenomenon is analyzed by using the Cattaneo-Christov theory. By applying the appropriate similarity transformations, the governing equations of motion turn into a set of nonlinear differential equations. For the velocity, temperature, and concentration fields, the resultant equations are then solved as series solutions using the homotopy analysis approach. Using graphical representations, the physical behavior of significant factors is examined in depth. The analysis reveals that higher Maxwell parameter values reduce the flow field while increasing energy transportation in the fluid flow. Further, it is noted that thermal distribution declines for the higher values of the thermal relaxation parameter. Additionally, the solutal distribution bootup for the increasing values of Schmidt number while it shows a decreasing trend for homogeneous and heterogeneous reactions strength. In order to verify our findings, a comparison to earlier research is also included.

1. Introduction

The numerous fluid models with distinct dynamical features induced by stretching geometries attract investigators to analyze their attributes in the field of engineering because of their wide range of applications such as glass fiber, wire drawing, hot rolling, and paper production. In extrusion forms, the study of flow and heat transport phenomena caused by the stretching cylinder is extremely important. Majeed et al. [1] explored the analysis of the heat transport caused by a stretching cylinder with partial slip and specified surface heat flux. Mahdy [2] discussed the flow and heat transportation of a Casson fluid due to a stretching cylinder with Dufour and Soret effects. Alamri et al. [3] studied the effects of mass transfer on magneto second-grade fluid flow over a stretching cylinder using the innovative perspective of the Cattaneo-Christov heat transport. Singh et al. [4] scrutinized the melting transport assessment on magnetic nanofluid flow across a stretching cylinder. Song et al. [5] discussed the effects of the gyrotactic microorganisms on Sutterby nanofluid with melting heat transport. Mathematical modeling for the time-dependent flow of Oldroyd-B material with energy transport induced by stretching cylinder was interpreted by Yasir et al. [6]. Farooq et al. [7] discussed the physical properties and heat transport of the bioconvective flow of Casson nanofluid. The latest studies on stretching cylinder can be found in Refs. [8–20]).

* Corresponding authors.
E-mail addresses: myasir@math.qau.edu.pk (M. Yasir), mkhan@qau.edu.pk (M. Khan).

https://doi.org/10.1016/j.heliyon.2023.e19004
Received 5 February 2023; Received in revised form 3 August 2023; Accepted 4 August 2023
Available online 6 August 2023

Nomenclature

u, w	velocity component $[ms^{-1}]$
c	stretching rate $[s^{-1}]$
T	fluid temperature $[K]$
λ_1	relaxation time $[s]$
c_p	specific heat $[JK^{-1}m^{-3}]$
ν	kinematic viscosity $[m^2s^{-1}]$
μ	dynamic viscosity $[pa.\ s]$
k	thermal conductivity $[Wm^{-1}K^{-1}]$
α	thermal diffusivity $[m^2s^{-1}]$
ρ_f	fluid density $[kgm^{-3}]$
T_∞	ambient temperature $[K]$
k_c	homogeneous species
k_s	heterogeneous species
Pr	Prandtl number
γ	curvature parameter
S	unsteadiness parameter
Sc	Schmidt number
λ^*	diffusion coefficient
σ	electrical conductivity
M	magnetic field parameter
K_s	heterogeneous reaction
K	homogeneous reaction
f	dimensionless stream function
θ	dimensionless temperature
g	dimensionless concentration
a_o	positive constant

The analysis of heat and mass transport acquired too much attention from researchers due to its numerous applications in engineering. The basic mathematical principles of Fourier's and Fick's laws are applied to explain the mechanisms of the transportation of heat and mass in any medium as a result of thermal and solutal differences, respectively. According to Fourier's law [21], the temperature field can be expressed as a parabolic-type equation, which means that heat transfer occurs at an infinitely fast speed and propagates throughout the medium with initial disruption. To fix this problem, Fourier's law required some modifications. There have been numerous attempts to settle this conundrum, while none have been at all successful. In order to produce the hyperbolic-type equation for the heat transport phenomenon, Cattaneo [22] adjusted Fourier's law by counting the thermal relaxation time. It is known as the Maxwell-Cattaneo model. Christov [23] modified the MC model by covering the time derivative. After that, to study the flow of both Newtonian and non-Newtonian fluids in various geometries, scientists used the Cattaneo-Christov double diffusion theory, see Refs. [24–33].

The study of chemical reactions in fluid mechanics has received a lot of interest. The importance of these flows may be seen in numerous processes like polymer synthesis, hydrometallurgical industries, food processing, fog creation and dispersion, ceramics, and freezing effects in crop damage. In chemical processes, both homogeneous and heterogeneous types of reactions occur. In the case of homogeneous reactions, consistent involvement of reactions happens across the entire required stage, and in the case of heterogeneous reactions, it appears in a confined border or within the specified region. Various chemical processes incorporate both homogeneous and heterogeneous reactions. Chaudhary and Merkin have proposed homogenous-heterogeneous reactions with the same diffusivities [34]. The viscous fluid flow with homogeneous-heterogeneous reactions through a flat plate was studied by Merkin [35]. Hamid [36] conducted a numerical analysis of the outcomes of thermal conductivity and catalytic effects on Williamson fluid flow. In the three-dimensional flow of Cross fluid, Ali et al. [37] examined the characteristics of homogeneous-heterogeneous reactions and generalized Fourier's heat flux. Khan et al. [38] investigated the temperature-dependent heat source/sink effects in unsteady stagnation-point flow of MHD Oldroyd-B fluid with cubic autocatalysis chemical reaction. The valuable contribution on flow and heat transport with homogeneous-heterogeneous chemical reactions can be found in Refs. [39–45].

The goal of this study is to scrutinize the viscoelastic fluid flow caused by stretching cylinder under the influence of homogeneous-heterogeneous processes. The modified Fourier law is employed for the thermal transport of the Maxwell fluid flow. As a result, we produced a mathematical model in the form of partial differential equations for the time-dependent flow of magnetized Maxwell fluid. With appropriate transformations, the controlling PDEs are turned into non-linear ordinary differential systems. The resultant equations are then solved as series solutions using the homotopy analysis approach. The results for the velocity, thermal, and concentration fields are graphically presented and scrutinized in detail using physical justification.

2. Problem formulation

Here we consider the unsteady axisymmetric flow of Maxwell fluid due to the stretching cylinder, having a radius of R. The surface of the cylinder is physically stretched with a velocity $u_w\left(=\frac{cz}{1-\delta t}\right)$ where $c, \delta(>0)$. As shown in Fig. 1, we formulated the physical phenomenon in cylindrical polar coordinates, by assuming u and w are, respectively, $z-$ axis and $r-$ axis velocity components. The mechanism of thermal transport in the flow of Maxwell fluid is modeled by using thermal relaxation effects. Further, the solutal transport phenomenon of the flow is studied by considering the homogeneous-heterogeneous reactions.

The following homogeneous-heterogeneous reaction model is used [34]:

$$\alpha^* + 2\beta^* \rightarrow 3\beta^*, \text{rate} = k_c a b^2 \tag{1}$$

on the catalyst surface, the isothermal reaction is illustrated as

$$\alpha^* \rightarrow \beta^*, \text{rate} = k_s a \tag{2}$$

where α^* and β^* signify autocatalysts of the chemical reactions, a and b describe the concentration of chemical reaction, and k_c and k_s denoted the reaction constants. According to Cattaneo-Christov theory, heat flux is given [33]:

$$\mathbf{q} + \lambda_t \left[\frac{\partial \mathbf{q}}{\partial t} - \mathbf{q}.\nabla\mathbf{V} + \mathbf{V}.\nabla\mathbf{q} + (\nabla.\mathbf{V})\,\mathbf{q}\right] = -k\nabla T \tag{3}$$

in which $\mathbf{q}$ the heat flux, λ_t the thermal relaxation, $\mathbf{V}$ the velocity field, k thermal conductivity. For $\lambda_t = 0$ the above equations reduce to classical Fourier law

$$\mathbf{q} + \lambda_t \left[\frac{\partial \mathbf{q}}{\partial t} + \mathbf{V}.\nabla\mathbf{q} - \mathbf{q}.\nabla\mathbf{V}\right] = -k\nabla T \tag{4}$$

Under the above consideration, the model equations are [38,46]:

$$\frac{\partial(ru)}{\partial z} + \frac{\partial(rw)}{\partial r} = 0 \tag{5}$$

$$\begin{aligned}\frac{\partial u}{\partial t} + u\frac{\partial u}{\partial z} + w\frac{\partial u}{\partial r} + \lambda_1\left\{\frac{\partial^2 u}{\partial t^2} + u^2\frac{\partial^2 u}{\partial z^2} + w^2\frac{\partial^2 u}{\partial r^2} + 2u\frac{\partial^2 u}{\partial t\partial z} + 2w\frac{\partial^2 u}{\partial t\partial r} + 2uw\frac{\partial^2 u}{\partial r\partial z}\right\} \\ = \nu\left(\frac{\partial^2 u}{\partial r^2} + \frac{1}{r}\frac{\partial u}{\partial r}\right) - \frac{\sigma B_o^2}{\rho_f}\left\{u + \lambda_1\left(\frac{\partial u}{\partial t} + w\frac{\partial u}{\partial r}\right)\right\}\Bigg\}\end{aligned} \tag{6}$$

$$\frac{\partial T}{\partial t} + u\frac{\partial T}{\partial z} + w\frac{\partial T}{\partial r} + \lambda_t\left\{\begin{array}{l}\dfrac{\partial^2 T}{\partial t^2} + \dfrac{\partial u}{\partial t}\dfrac{\partial T}{\partial z} + 2u\dfrac{\partial^2 T}{\partial t\partial z} + \dfrac{\partial w}{\partial t}\dfrac{\partial T}{\partial r} + 2w\dfrac{\partial^2 T}{\partial t\partial r} \\ +2uw\dfrac{\partial^2 T}{\partial r\partial z} + w^2\dfrac{\partial^2 T}{\partial r^2} + u^2\dfrac{\partial^2 T}{\partial z^2} + u\dfrac{\partial u}{\partial z}\dfrac{\partial T}{\partial z} \\ +w\dfrac{\partial u}{\partial r}\dfrac{\partial T}{\partial z} + u\dfrac{\partial w}{\partial z}\dfrac{\partial T}{\partial r} + w\dfrac{\partial w}{\partial r}\dfrac{\partial T}{\partial r}\end{array}\right\} = \frac{\alpha}{r}\frac{\partial}{\partial r}\left(r\frac{\partial T}{\partial r}\right), \tag{7}$$

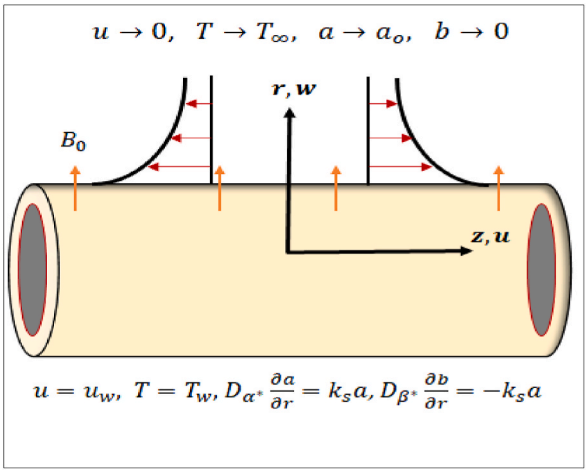

Fig. 1. Geometry of the problem.

$$\frac{\partial a}{\partial t}+u\frac{\partial a}{\partial z}+w\frac{\partial a}{\partial r}=D_{\alpha^*}\left(\frac{1}{r}\frac{\partial a}{\partial r}+\frac{\partial^2 a}{\partial r^2}\right)-k_c ab^2, \tag{8}$$

$$\frac{\partial b}{\partial t}+u\frac{\partial b}{\partial z}+w\frac{\partial b}{\partial r}=D_{\beta^*}\left(\frac{1}{r}\frac{\partial b}{\partial r}+\frac{\partial^2 b}{\partial r^2}\right)+k_c ab^2, \tag{9}$$

with BCs

$$\left.\begin{array}{l} u=u_w\ w=0, T=T_w, \\ D_{\alpha^*}\dfrac{\partial a}{\partial r}=k_s a, D_{\beta^*}\dfrac{\partial b}{\partial r}=-k_s a \\ u\to 0, T\to T_\infty, a\to a_o, b\to 0 \ \text{ as } \ r\to\infty \end{array}\right\} \text{at } \ r=R \tag{10}$$

By letting:

$$\left.\begin{array}{l} u=\dfrac{cz}{1-\delta t}f'(\eta), w=-\dfrac{R}{r}\sqrt{\dfrac{c\nu}{1-\delta t}}f(\eta), \theta=\dfrac{T-T_\infty}{T_w-T_\infty}, \\ a=a_o g(\eta), b=a_o h(\eta), \eta=\sqrt{\dfrac{c}{\nu(1-\delta t)}}\left(\dfrac{r^2-R^2}{2R}\right) \end{array}\right\} \tag{11}$$

we have

$$\begin{aligned} &(1+2\eta\gamma)f'''+2\gamma f''+ff''-f'^2-Sf'-\frac{1}{2}\eta Sf''-\frac{De_1\gamma}{(1+2\eta\gamma)}f^2f'' \\ &+De_1\left\{\begin{array}{l} 2ff'f''-2Sf'^2-2S^2f'-\eta Sf'f''+3Sff''-f^2f''' \\ +\eta Sff'''-\dfrac{7}{4}\eta S^2f''-\dfrac{1}{4}\eta^2S^2f''' \end{array}\right\} \\ &\left.\begin{array}{l} -M\left(f'+\dfrac{De_1}{2}\eta Sf''+De_1Sf'-De_1ff''\right)=0, \end{array}\right\}, \end{aligned} \tag{12}$$

$$\begin{aligned} &(1+2\eta\gamma)\theta''+2\gamma\theta'+\Pr f\theta'-\frac{1}{2}\Pr\eta S\theta' \\ &-\Pr\beta_t\left(\frac{3}{4}\eta S^2\theta'-\frac{3}{2}Sf\theta'-\frac{1}{2}\eta Sf'\theta'+\frac{1}{4}\eta^2S^2\theta''-\eta Sf\theta''+f^2\theta''+ff'\theta'\right)=0\Big\}, \end{aligned} \tag{13}$$

$$(1+2\eta\gamma)\,g''+2\gamma g'+Scfg'-\frac{1}{2}\eta SScg'-ScKgh^2=0 \tag{14}$$

$$\lambda^*(1+2\eta\gamma)\,h''+2\gamma\lambda^*h'+Scfh'-\frac{1}{2}\eta SSch'+ScKgh^2=0 \tag{15}$$

with relevant boundary conditions

$$\left.\begin{array}{l} f(0)=0, f'(0)=1, \theta(0)=1, g'(0)=K_s g(0), \lambda^* h'(0)=-K_s g(0), \\ f'(\infty)=0, \theta(\infty)=0, g(\infty)=1, h(\infty)=0 \end{array}\right\} \tag{16}$$

In the above equations, $\gamma\left(=\frac{1}{R}\sqrt{\frac{\nu(1-\delta t)}{c}}\right)$ is the curvature parameter, $De_1\left(=\frac{\lambda_1 c}{1-\delta t}\right)$ the Deborah number, $S\left(=\frac{\delta}{c}\right)$ the unsteadiness parameter, $M\left(=\sqrt{\frac{\sigma B_o^2(1-\delta t)}{c\rho_f}}\right)$ the magnetic parameter $\Pr\left(=\frac{\nu}{\alpha}\right)$ the Prandtl and $Sc\left(=\frac{\nu}{D_{\alpha^*}}\right)$ the Schmidt number, $K_s\left(=\frac{k_s}{D_{\alpha^*}}\sqrt{\frac{\nu(1-\delta t)}{c}}\right)$ is the strength of heterogeneous reaction, $\beta_t\left(=\frac{\lambda_1 c}{1-\delta t}\right)$ the thermal relaxation parameter, $K\left(=\frac{k_c(1-\delta t)\,a_o^2}{c}\right)$ is the strength of homogeneous reaction, $\lambda^*\left(=\frac{D_{\beta^*}}{D_{\alpha^*}}\right)$ the ratio of the diffusion coefficient.

Assume D_{α^*} and D_{β^*} are equivalent, i.e., $\lambda^*(=1)$, so

$$g(\eta)+h(\eta)=1. \tag{17}$$

from equation (14) and (15), we have

$$(1+2\eta\gamma)\,g''+2\gamma g'+Scfg'-\frac{1}{2}\eta SScg'-KgSc(1-g)^2=0 \tag{18}$$

$$g(\eta) \to 1, g^{'}(0) = K_s g(0), \text{as } \eta \to \infty. \tag{19}$$

3. Homotopic solution

The auxiliary linear operators are as follows [47,48]:

$$f_o(\eta) = 1 - e^{-\eta},\ \theta_o(\eta) = e^{-\eta} \text{ and } g_o(\eta) = 1 - \frac{1}{2}e^{-\eta k_s} \tag{20}$$

$$\mathbf{L}_f(\eta) = \frac{\partial^3 f}{\partial \eta^3} - \frac{\partial f}{\partial \eta},\ \mathbf{L}_\theta(\eta) = \frac{\partial^2 \theta}{\partial \eta^2} - \theta \text{ and } \mathbf{L}_g(\eta) = \frac{\partial^2 g}{\partial \eta^2} - g \tag{21}$$

satisfying

$$\left.\begin{array}{l} \mathbf{L}_f\left[\alpha_0^* + \alpha_1^* e^{\eta} + \alpha_2^* e^{-\eta}\right] = 0 \\ \mathbf{L}_\theta\left[\alpha_3^* e^{\eta} + \alpha_4^* e^{-\eta}\right] = 0 \\ \mathbf{L}_g\left[\alpha_5^* e^{\eta} + \alpha_6^* e^{-\eta}\right] = 0 \end{array}\right\} \tag{22}$$

where $\alpha_i^* (i = 0, 1, .., 6)$ are the constants.

4. Convergence analysis

The convergence of the analytic solutions depends heavily on $\hbar_f$, $\hbar_\theta$, and $\hbar_g$. The $\hbar-$ curves are thus displayed at the 13*th* order of approximations, see Fig. 2. The acceptable ranges for auxiliary parameters are $-1.23 \le \hbar_f \le -0.09$, $-1.47 \le \hbar_\theta \le -0.31$ and $-1.47 \le \hbar_\varphi \le -0.13$. The analytic series solutions converges in the entire range of $\eta (0 \le \hbar \le \infty)$ when $\hbar_f = -1$, $\hbar_\theta = -1.1$, and $\hbar_g = -1.4$.

5. Discussion of results

The flow behavior, thermal and solutal transport of unsteady Maxwell fluid induced by stretching cylinder is described by the governing equations (12) to (16), and are analyzed and discussed in this section. To understand the physical conduct of these outcomes, the physical parameters are detected in the range: $S(0.1 \le S \le 0.4)$, $\gamma(0.0 \le \gamma \le 0.3)$, $De_1(0.1 \le De_1 \le 0.7)$, $\Pr(6.5 \le \Pr \le 7.1)$, $\beta_t(0.1 \le \beta_t \le 0.4)$, $M(0.1 \le M \le 0.4)$, and $Sc(1.0 \le Sc \le 2.5)$, $Ks(0.3 \le K_s \le 0.9)$, and $K(0.5 \le K \le 2.0)$ and for which the graphical results satisfy the far field boundary conditions. The consequence of the unsteadiness parameter S on fluid velocity, thermal and solutal distributions are depicted in Fig. 3(a) to 3(c). These figures clearly illustrate that increasing the unsteadiness parameter S increases the fluid velocity and heat distribution, while opposite results are observed for concentration fields. The outcomes of curvature parameter γ on the velocity, thermal, and solutal distributions are examined in Fig. 4(a) to 4(c), respectively. In these plots, we observed an increasing trend for the increasing values of γ. Because, increasing the value of γ diminishes the radius of the cylinder, reducing the role of the boundary in fluid motion. As a result, the velocity of the fluid enhances which improves the thermal and solutal distributions. The influence of Maxwell parameter De_1 declines the fluid velocity and boosts the thermal distribution, as depicted in Fig. 5(a) and (b), respectively. Physically, the rheology of a material of the viscoelastic type is described by the Maxwell parameter De_1. The dimensionless relaxation time is defined by the Maxwell parameter De_1. The relaxation time is used to represent the phenomenon of stress relaxation caused by the material's elasticity. The material therefore behaves like a solid for larger values of De_1. It signifies that the material needs a longer time to hold its deformation, and as a result, a higher value of De_1 causes a decrease in fluid velocity. On the

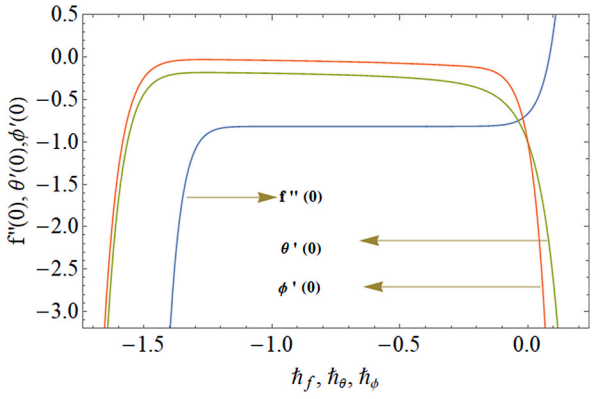

Fig. 2. The $\hbar$ curves.

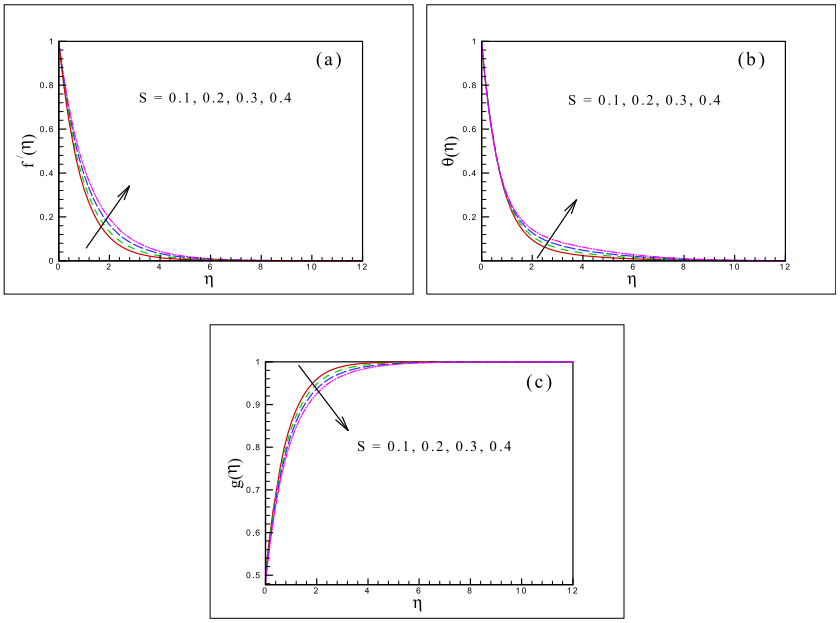

Fig. 3. (a–c): Plot of $f'(\eta)$, $\theta(\eta)$ and $g(\eta)$ for S.

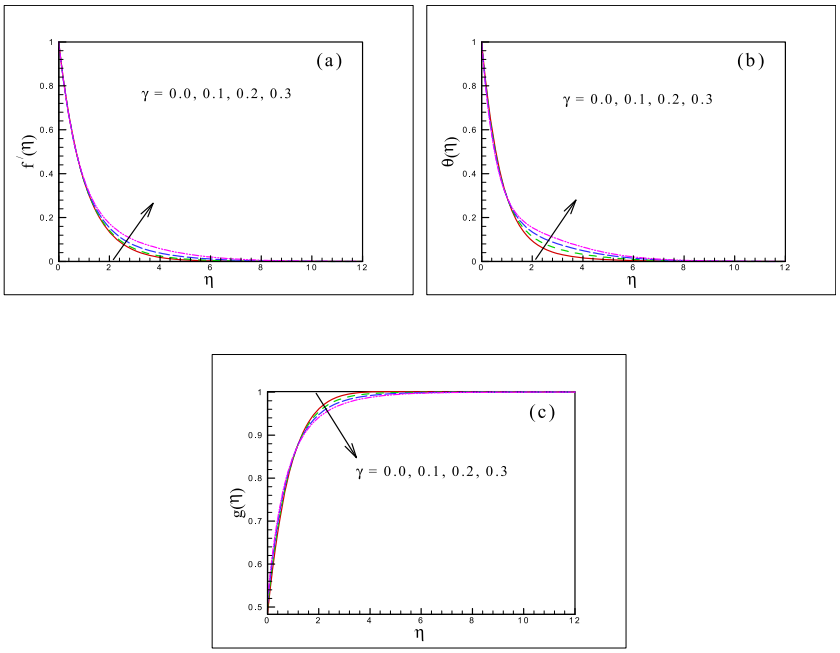

Fig. 4. (a–c): Plot of $f'(\eta)$, $\theta(\eta)$ and $g(\eta)$ for γ.

other hand, an upgrade in heat conduction causes the energy transport phenomena to increase for the same trend of De_1. Fig. 6(a) and (b) is presented to illustrate how the thermal relaxation time parameter β_t and the Prandtl number Pr affect temperature distribution. According to the assessment, increased values of β_t and Pr lead to a decrease in the temperature distribution of Maxwell fluid. The reason for this is that increasing the values of the thermal relaxation time parameter needs more time for heat conduction, resulting in a fall in fluid temperature. Further, the thermal diffusivity of a liquid, which decreases as Prandtl number values increase, is inversely related to Prandtl number. As a result of the reduced thermal diffusivity of the liquid, the temperature of the Maxwell fluid falls. The effects of magnetic fields on velocity and temperature fields are shown in Fig. 7(a) and (b), respectively. In terms of physics, the magnetic field's influence on the Lorentz force increases as M increases. The fluid's velocity decreases as a result of the force's resistance to the flow of the fluid. As the Lorentz force increases, on the other side, the energy conduction between fluid particles

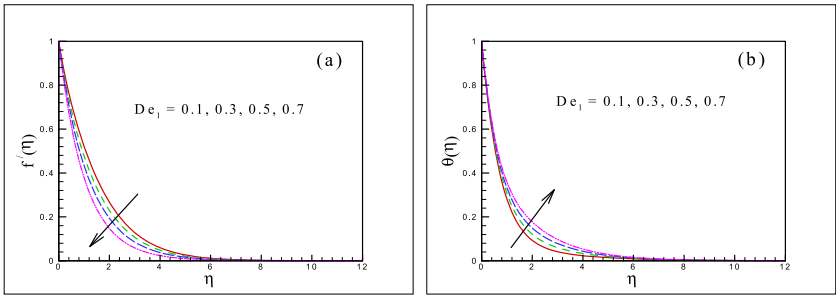

Fig. 5. (a–b): Plot of $f'(\eta)$ and $\theta(\eta)$ for De_1.

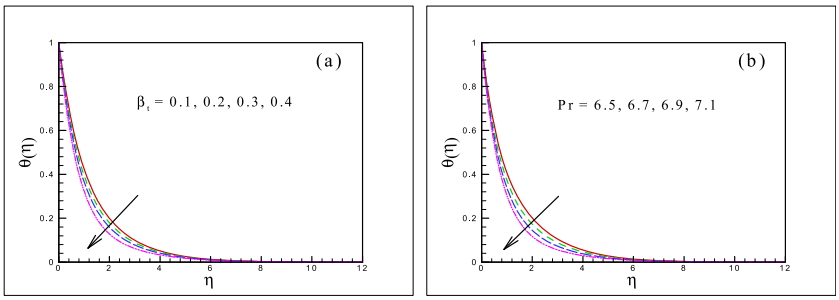

Fig. 6. (a–b): Plot of $\theta(\eta)$ for β_t and Pr.

increases. Fig. 8 characterizes the impact of Schmidt number *Sc* on the solutal field. The behavior of concentration improves as the Schmidt number increases. Schmidt number is the relationship between momentum and mass diffusivity. Here, larger Schmidt number values are associated with small diffusivity, resulting in an increase in solutal field. Fig. 9(a) depicts the effect of the strength of the heterogeneous reaction parameter *Ks* on the concentration distribution. As the values of the heterogeneous parameter *Ks* strength increase, the concentration profile declines. In Fig. 9(b), it is depicted how the parameter *K* affects the concentration distribution. For the increasing strength of *K*, the concentration profile diminishes. To ensure the validity of our findings, a comparison for reduced $-f''(0)$ with various De_1 values is provided in Table 1.

6. Concluding remarks

The key points are as follows in light of the findings of the analysis and discussion:

- The unsteadiness and curvature parameters enhanced the velocity profile and thermal distributions of the Maxwell fluid.
- As the Maxwell parameter increases, the flow field was decreased while the heat distribution was increased.
- Temperature fields dropped as the Prandtl number increased.
- The concentration profile declined as the homogenous and heterogeneous reactions parameter strength increased.
- The thermal curves diminished as a result of increasing thermal relaxation parameter.

Author contribution statement

Muhammad Yasir: Conceived and designed the analysis; Wrote the paper.
Masood Khan, M. Munawwar Iqbal Ch: Conceived and designed the analysis; Analyzed and interpreted the data.
Asia Anjum: Analyzed and interpreted the data; Contributed analysis tools or data.

Data availability statement

The data that has been used is confidential.

Declaration of competing interest

The authors declare that they have no known competing financial interests or personal relationships that could have appeared to influence the work reported in this paper.

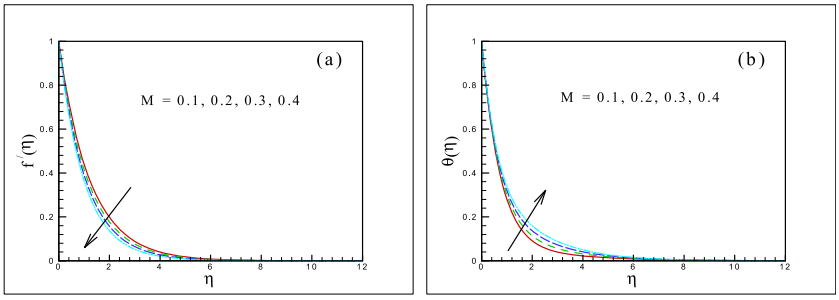

Fig. 7. (a–b): Plot of $f'(\eta)$ and $\theta(\eta)$ for M.

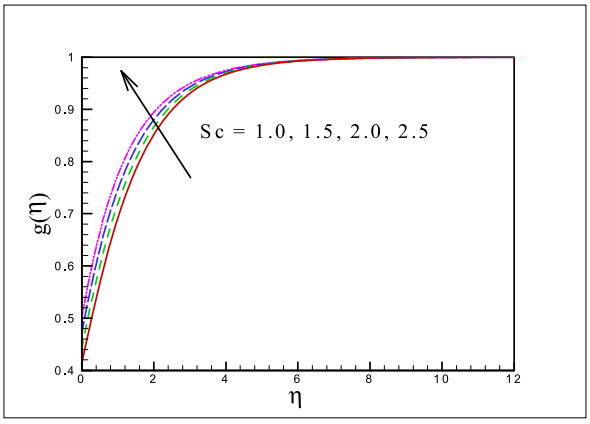

Fig. 8. Plot of $g(\eta)$ for Sc.

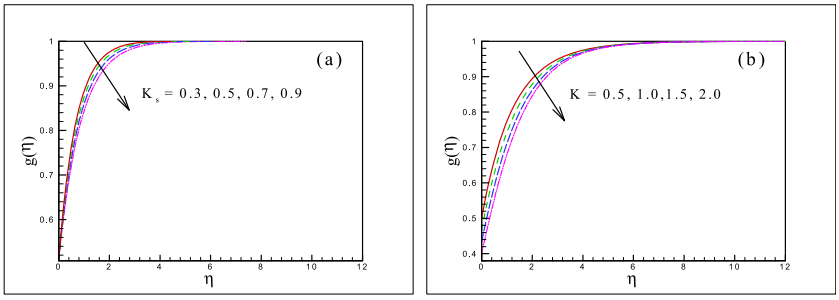

Fig. 9. (a–b): Plot of $g(\eta)$ for K_s and K.

Table 1
Comparison of $-f''(0)$ for De_1 when $\gamma = S = 0$.

De_1	Abel et al. [49]	Waqas et al. [50]	Present results
0.0	1.00000	1.00000	1.00000
0.2	1.05194	1.05188	1.05171
0.4	1.10185	1.10190	1.10157
0.6	1.15016	1.15013	1.15044
0.8	1.19669	1.19671	1.19608

References

[1] A. Majeed, T. Javed, A. Ghaffari, M.M. Rashidi, Analysis of heat transfer due to stretching cylinder with partial slip and prescribed heat flux: a Chebyshev Spectral Newton Iterative Scheme, Alex. Eng. J. 54 (4) (2015) 1029–1036.
[2] A. Mahdy, Heat transfer and flow of a Casson fluid due to a stretching cylinder with the Soret and Dufour effects, J. Eng. Phys. Thermophys. 88 (2015) 928–936.

[3] S.Z. Alamri, A.A. Khan, M. Azeez, R. Ellahi, Effects of mass transfer on MHD second grade fluid towards stretching cylinder: a novel perspective of Cattaneo–Christov heat flux model, Phys. Lett. 383 (2–3) (2019) 276–281.

[4] K. Singh, A.K. Pandey, M. Kumar, Melting heat transfer assessment on magnetic nanofluid flow past a porous stretching cylinder, J. Egypt. Math. Soc. 29 (2021) 1–14.

[5] Y.Q. Song, H. Waqas, K. Al-Khaled, U. Farooq, S.U. Khan, M.I. Khan, Y.M. Chu, S. Qayyum, Bioconvection analysis for Sutterby nanofluid over an axially stretched cylinder with melting heat transfer and variable thermal features: a Marangoni and solutal model, Alex. Eng. J. 60 (5) (2021) 4663–4675.

[6] M. Yasir, A. Ahmed, M. Khan, A.K. Alzahrani, Z.U. Malik, A.M. Alshehri, Mathematical modelling of unsteady Oldroyd-B fluid flow due to stretchable cylindrical surface with energy transport, Ain Shams Eng. J. 14 (1) (2023), 101825.

[7] U. Farooq, H. Waqas, S.E. Alhazmi, A. Alhushaybari, M. Imran, R. Sadat, T. Muhammad, M.R. Ali, Numerical treatment of Casson nanofluid bioconvectional flow with heat transfer due to stretching cylinder/plate: variable physical properties, Arab. J. Chem. (2023), 104589, https://doi.org/10.1016/j.arabjc.2023.104589.

[8] G. Kotha, V.R. Kolipaula, M.V.S. Rao, S. Penki, A.J. Chamkha, Internal heat generation on bioconvection of an MHD nanofluid flow due to gyrotactic microorganisms, Eur. Phys. J. Plus 135 (2020) 1–19.

[9] K. Gangadhar, K.B. Lakshmi, T. Kannan, A.J. Chamkha, Bioconvective Magnetized Oldroyd-B Nanofluid Flow in the Presence of Joule Heating with Gyrotactic Microorganisms, Waves Random Complex Media, 2022, pp. 1–21, https://doi.org/10.1080/17455030.2022.2050441.

[10] I.A. Shah, S. Bilal, A. Riaz, E.M.T. El-Din, M.M. Alqarni, H. Hamam, Thermosolutal natural convective transport in Casson fluid flow in star corrugated cavity with Inclined magnetic field, Results Phys. 43 (2022), 106081.

[11] K. Gangadhar, M.A. Kumari, A.J. Chamkha, EMHD flow of radiative second-grade nanofluid over a Riga Plate due to convective heating: revised Buongiorno's nanofluid model, Arabian J. Sci. Eng. 47 (7) (2022) 8093–8103.

[12] Z. Hussain, A. Hussain, M.S. Anwar, M. Farooq, Analysis of Cattaneo–Christov heat flux in Jeffery fluid flow with heat source over a stretching cylinder, J. Therm. Anal. Calorim. 147 (2022) 1–12.

[13] K. Gangadhar, K.B. Lakshmi, S. El-Sapa, M.V.S. Rao, A.J. Chamkha, Thermal Energy Transport of Radioactive Nanofluid Flow Submerged with Microorganisms with Zero Mass Flux Condition, Waves Random Complex Media, 2022, pp. 1–23, https://doi.org/10.1080/17455030.2022.2072536.

[14] J. Yin, X. Zhang, M.I.U. Rehman, A. Hamid, Thermal radiation aspect of bioconvection flow of magnetized Sisko nanofluid along a stretching cylinder with swimming microorganisms, Case Stud. Therm. Eng. 30 (2022), 101771.

[15] J. Alam, M.G. Murtaza, E. Tzirtzilakis, M. Ferdows, MagnetoHydrodynamic and FerroHydrodynamic interactions on the biomagnetic flow and heat transfer containing magnetic particles along a stretched cylinder, Eur. J. Comput. Mech. 31 (1) (2022) 1–40.

[16] K. Gangadhar, M.A. Kumari, M.V.S. Rao, A.J. Chamkha, Oldroyd-B nanoliquid flow through a triple stratified medium submerged with gyrotactic bioconvection and nonlinear radiations, Arabian J. Sci. Eng. 47 (2022) 8863–8875.

[17] Y.D. Reddy, B.S. Goud, K.S. Nisar, B. Alshahrani, M. Mahmoud, C. Park, Heat absorption/generation effect on MHD heat transfer fluid flow along a stretching cylinder with a porous medium, Alex. Eng. J. 64 (2023) 659–666.

[18] S. Bilal, N.Z. Khan, I. Fatima, A. Riaz, G.J. Ansari, S.E. Alhazmi, E.M. El-Din, Mixed convective heat transfer in a power-law fluid in a square enclosure: higher order finite element solutions, Front. Physiol. 10 (2023) 1327.

[19] T. Hayat, A. Razaq, S.A. Khan, A. Alsaedi, Entropy generation in chemically reactive and radiative Reiner-Rivlin fluid flow by stretching cylinder, J. Magn. Magn Mater. 573 (2023), 170657.

[20] S. Bilal, A. Ullah, I.A. Shah, M.I. Asjad, M.Y. Almusawa, S.M. Eldin, Analysis of free and forced convections in the flow of radiative viscous fluid with oxytactic microorganisms, Front. Mater. 10 (2023), 1138313.

[21] J.B.J. Fourier, Theorie analytique de la chaleur, Didot, Paris, 1822, pp. 499–508.

[22] C. Cattaneo, Sulla conduzione del calore, Atti Sem. Mat. Fis. Univ. Modena 3 (1948) 83–101.

[23] C.I. Christov, On frame indifferent formulation of the Maxwell–Cattaneo model of finite-speed heat conduction, Mech 36 (4) (2009) 481–486.

[24] B. Ramandevi, J.R. Reddy, V. Sugunamma, N. Sandeep, Combined influence of viscous dissipation and non-uniform heat source/sink on MHD non-Newtonian fluid flow with Cattaneo-Christov heat flux, Alex. Eng. J. 57 (2) (2018) 1009–1018.

[25] M.I. Khan, F. Alzahrani, Transportation of heat through Cattaneo-Christov heat flux model in non-Newtonian fluid subject to internal resistance of particles, Appl. Math. Mech. 41 (2020) 1157–1166.

[26] F.O.M. Mallawi, M. Bhuvaneswari, S. Sivasankaran, S. Eswaramoorthi, Impact of double-stratification on convective flow of a non-Newtonian liquid in a Riga plate with Cattaneo-Christov double-flux and thermal radiation, Ain Shams Eng. J. 12 (1) (2021) 969–981.

[27] K.G. Kumar, M.G. Reddy, M.V.V.N.L. Sudharani, S.A. Shehzad, A.J. Chamkha, Cattaneo–Christov heat diffusion phenomenon in Reiner–Philippoff fluid through a transverse magnetic field, Phys. A: Stat. Mech. Appl. 541 (2020), 123330.

[28] M.I. Khan, M. Nigar, T. Hayat, A. Alsaedi, On the numerical simulation of stagnation point flow of non-Newtonian fluid (Carreau fluid) with Cattaneo-Christov heat flux, Comput. Methods Progr. Biomed. 187 (2020), 105221.

[29] A. Salmi, H.A. Madkhali, B. Ali, M. Nawaz, S.O. Alharbi, A.S. Alqahtani, Numerical study of heat and mass transfer enhancement in Prandtl fluid MHD flow using Cattaneo-Christov heat flux theory, Case Stud. Therm. Eng. 33 (2022), 101949.

[30] M. Yasir, M. Khan, A. Ahmed, M. Sarfraz, Flow of Oldroyd-B Nanofluid in Non-inertial Frame Inspired by Cattaneo-Christov Theory, Waves Random Complex Media, 2023, pp. 1–12, https://doi.org/10.1080/17455030.2023.2172626.

[31] M. Ramzan, U. Shamshad, S. Rehman, M.S. Junaid, A. Saeed, P. Kumam, Analytical simulation of Hall current and Cattaneo–Christov heat flux in cross-hybrid nanofluid with autocatalytic chemical reaction: an engineering application of engine oil, Arabian J. Sci. Eng. 48 (3) (2023) 3797–3817.

[32] R.P. Gowda, R.N. Kumar, R. Kumar, B.C. Prasannakumara, Three-dimensional coupled flow and heat transfer in non-Newtonian magnetic nanofluid: an application of Cattaneo-Christov heat flux model, J. Magn. Magn Mater. 567 (2023), 170329.

[33] M. Yasir, M. Khan, Dynamics of heat transport in flow of non-linear Oldroyd-B fluid subject to non-Fourier's theory, ZAMM Z. fur Angew. Math. Mech. (2023), e202100393, https://doi.org/10.1002/zamm.202100393.

[34] M.A. Chaudhary, J.H. Merkin, A simple isothermal model for homogeneous-heterogeneous reactions in boundary-layer flow. I Equal diffusivities, Fluid Dynam. Res. 16 (6) (1995) 311.

[35] J.H. Merkin, A model for isothermal homogeneous-heterogeneous reactions in boundary-layer flow, Math. Comput. Model. Dyn. Syst. 24 (8) (1996) 125–136.

[36] A. Hamid, Numerical study of temperature dependent thermal conductivity and homogeneous-heterogeneous reactions on Williamson fluid flow, J. Phys. Commun. 4 (8) (2020), 085009.

[37] M. Ali, F. Sultan, W.A. Khan, M. Shahzad, H. Arif, M. Irfan, Characteristics of generalized Fourier's heat flux and homogeneous-heterogeneous reactions in 3D flow of non-Newtonian cross fluid, Int. J. Numer. Methods Heat Fluid Flow 31 (11) (2021) 3304–3318.

[38] M. Khan, M. Yasir, A.S. Alshomrani, S. Sivasankaran, Y.R. Aladwani, A. Ahmed, Variable heat source in stagnation-point unsteady flow of magnetized Oldroyd-B fluid with cubic autocatalysis chemical reaction, Ain Shams Eng. J. 13 (3) (2022), 101610.

[39] M. Waqas, Chemical reaction impact in dual diffusive non-Newtonian liquid featuring variable fluid thermo-solutal attributes, Chem. Phys. Lett. 802 (2022), 139661.

[40] M.B. Ashraf, S.U. Haq, The Convective Flow of Carreau Fluid over a Curved Stretching Surface with Homogeneous-Heterogeneous Reactions and Viscous Dissipation, Waves Random Complex Media, 2022, pp. 1–15, https://doi.org/10.1080/17455030.2022.2032867.

[41] F. Alzahrani, R.P. Gowda, R.N. Kumar, M.I. Khan, Dynamics of thermosolutal Marangoni convection and nanoparticle aggregation effects on Oldroyd-B nanofluid past a porous boundary with homogeneous-heterogeneous catalytic reactions, J. Indian Chem. Soc. 99 (6) (2022), 100458.

[42] A. Naseem, A. Shafiq, F. Naseem, M.U. Farooq, Aspects of homogeneous heterogeneous reactions for nanofluid flow over a riga surface in the presence of viscous dissipation, Energies 15 (19) (2022) 6891.

[43] N.A. Shah, O.K. Koriko, K. Ramesh, T. Oreyeni, Rheology of bioconvective stratified Eyring-Powell nanofluid over a surface with variable thickness and homogeneous-heterogeneous reactions, Biomass Convers. Biorefin (2023) 1–17, https://doi.org/10.1007/s13399-023-04234-5.

[44] Z. Abbas, I. Mehdi, J. Hasnain, A.K. Alzahrani, M. Asma, Homogeneous-heterogeneous reactions in MHD mixed convection fluid flow between concentric cylinders with heat generation and heat absorption, Case Stud. Therm. Eng. 42 (2023), 102718.
[45] S. Rehman, S. Alqahtani, S. Alshehery, S.B. Moussa, A comprehensive physical insight of inclined magnetic field on the flow of generalized Newtonian fluid within a conduit with Homogeneous-heterogeneous reactions, Arab. J. Chem. 16 (5) (2023), 104633.
[46] M. Khan, A. Ahmed, M. Irfan, J. Ahmed, Analysis of Cattaneo–Christov theory for unsteady flow of Maxwell fluid over stretching cylinder, J. Therm. Anal. Calorim. 144 (2021) 145–154.
[47] S. Liao, Notes on the homotopy analysis method: some definitions and theorems, Commun. Nonlinear Sci. Numer. Simul. 14 (4) (2009) 983–997.
[48] S. Liao, On the relationship between the homotopy analysis method and Euler transform, Commun. Nonlinear Sci. Numer. Simul. 15 (6) (2010) 1421–1431.
[49] M.S. Abel, J.V. Tawade, M.M. Nandeppanavar, MHD flow and heat transfer for the upper-convected Maxwell fluid over a stretching sheet, Meccanica 47 (2012) 385–393.
[50] M. Waqas, M.I. Khan, T. Hayat, A. Alsaedi, Stratified flow of an Oldroyd-B nanoliquid with heat generation, Results Phys. 7 (2017) 2489–2496.